www.czasopisma.pan.pl PAN POLSKA AKADEMIA NAUK www.journals.pan.pl

PAN ARCHIVES OF ACOUSTICS
Vol. **45**, No. 3, pp. 433–444 (2020)
DOI: 10.24425/aoa.2020.134059

Research paper

Theoretical Analysis and Experimental Verification of Top Orthogonal to Bottom Arrays of Conducting Strips on Piezoelectric Slab

Yuriy TASINKEVYCH*, Ihor TROTS, Ryszard TYMKIEWICZ

Department of Ultrasound
Institute of Fundamental Technological Research
Polish Academy of Sciences
Pawinskiego 5B, 02-106 Warsaw, Poland
*Corresponding Author e-mail: yurijtas@ippt.pan.pl

(*received June 14, 2019; accepted March 13, 2020*)

The purpose of this work is to present a theoretical analysis of top orthogonal to bottom arrays of conducting electrodes of infinitesimal thickness (conducting strips) residing on the opposite surfaces of piezoelectric slab. The components of electric field are expanded into double periodic Bloch series with corresponding amplitudes represented by Legendre polynomials, in the proposed semi-analytical model of the considered two-dimensional (2D) array of strips. The boundary and edge conditions are satisfied directly by field representation, as a result. The method results in a small system of linear equations for unknown expansion coefficients to be solved numerically. A simple numerical example is given to illustrate the method. Also a test transducer was designed and a pilot experiment was carried out to illustrate the acoustic-wave generating capabilities of the proposed arrangement of top orthogonal to bottom arrays of conducting strips.

Keywords: boundary value problem; Fourier series; Bloch series; partial differential equations; piezoelectric transducer.

1. Introduction

Originally applied for surface acoustic wave (SAW) generation (White, Voltmer, 1965), periodic conducting strips applied on plane surface of solid (piezoelectric) body play an important role in many applications and in various fields like non-destructive testing (NDT) (Na *et al.*, 2008), microelectromechanical systems (MEMS) (Wang *et al.*, 2009), telecommunications (Fissi *et al.*, 2015), chemical sensing (Nguyen *et al.*, 2017), piezo-acoustics (Daniau *et al.*, 2004), and biotechnology (Senveli, Tigli, 2015; Danicki *et al.*, 2013). Different methods of analysis of periodic conducting strips were reported in literature from theoretical (Blotekjar *et al.*, 1973; Biryukov, Polevoi, 1996; Peach, 1981; Danicki, 1996) to purely numerical (Morgan, 1999; Bausk *et al.*, 2002). In (Blotekjar *et al.*, 1973) the problem of infinitely thin conducting strips on a dispersive semi-infinite dielectric solid was solved using electrostatic approximation and the electric filed solution was constructed as an infinite series of spatial harmonics. Analytical solution for surface electrostatic charge distribution, which characterizes well the most important parameters of such system of electrodes in practical applications, was derived for finite number of strips in (Biryukov, Polevoi, 1996) and for infinite periodic system of strips in (Peach, 1981). In (Danicki, 1996) spatial spectrum of the surface electrostatic charge distribution on strips was derived in analytical form for a finite number of strips. Numerical analysis mainly concerns the finite systems of conducting electrodes of arbitrary width and position. For example, in (Morgan, 1999) such system was approximated by an infinite periodic system of strips, where electrodes were modelled by connected strips and gaps (space between neighbouring electrodes) were modelled by the isolated ones. In (Bausk *et al.*, 2002) electrostatic problem for finite system of strips was formulated as a mixed boundary-value problem of the analytic function theory. Electrostatic charge distribution was expanded into the series of Chebyshev polynomials and its spatial spectrum was obtained then by numerical integration using Gauss formula.

The aim of current work is to present a theoretical analysis of the top orthogonal to bottom arrays of conducting strips sketched in Fig. 1. It is comprised of two orthogonal one-dimensional arrays of strips residing on the top and bottom surfaces of a piezoelectric slab. This can be considered as a two-dimensional (2D) generalization of the one-dimensional (1D) problem discussed above, which is a significant and important theoretical problem of the solid mechanics. Moreover, a practical aspect of the study of 2D arrays of conducting strips is that it can be suitable for modelling of novel design of 2D kerfless transducers (Chen *et al.*, 2014) used for example in ultrasound wave generation and detection instead of traditional matrices of piezoelectric elements (separated electrically and mechanically) (Seo, Yen, 2009).

In this work a semi-analytical method of analysis of the 2D array of strips residing on piezoelectric slab is presented (Fig. 1). Solutions for electrical and mechanical fields are sought in the form of double periodic Bloch series expansions satisfying the governing equations in piezoelectric slab. To obey periodic electric boundary conditions the amplitudes of Bloch components are represented by the series of Legendre polynomials, describing proper singular behaviour of the electric field in the vicinity of strips edges (Danicki, 2010).

The rest of the paper is organized as follows. In the next section the governing equations are briefly discussed. Mechanical and electrical boundary conditions are presented in Secs 3 and 4, respectively. Double series expansion of electric field components is presented in Sec. 5. A simple illustrative example presenting the method is shown in Sec. 6. In Sec. 7 experimental measurement of backscattered acoustic field using a test transducer is presented. Finally, in Sec. 8, conclusions of this work are summarized.

2. Governing equations

Consider a dielectric piezoelectric slab having its surfaces $x_3 = \pm h$ defined in the Cartesian coordinate system x_i, $i = 1, 2, 3$. Without loss of generality, piezoelectric material of the 2 mm symmetry class frequently used in applications (e.g. PZT and PVDF) will be considered. On the upper surface of the slab an infinite x_1-periodic system of conducting strips infinitely long in the x_2-direction is deposited. Similarly, on the bottom surface of the slab an infinite x_2-periodic system of infinitely long strips in the x_1-direction is deposited, as illustrated in Fig. 1.

To simplify the analysis the period Λ and the strip width w is assumed on both surfaces of the slab. The constitutive relations for piezoelectrics are:

$$\begin{aligned} T_{ij} &= c^E_{ijkl} S_{kl} - e_{kij} E_k, \\ D_i &= e_{ijk} S_{jk} + \epsilon^S_{ij} E_j, \end{aligned} \tag{1}$$

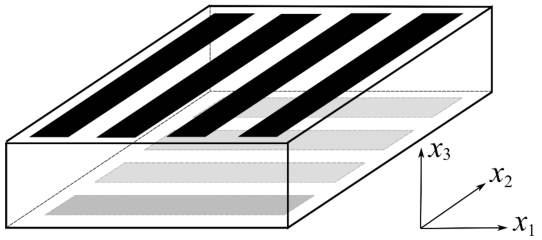

Fig. 1. Top orthogonal to bottom arrays of conducting strips residing on the opposite surfaces of piezoelectric dielectric slab.

and the corresponding system of governing equations can be written as:

$$\begin{aligned} c^E_{ijkl} u_{k,il} + e_{kij} \varphi_{,ik} &= \rho \ddot{u}_j, \\ e_{kij} u_{j,ik} - \epsilon^S_{ij} \varphi_{,ij} &= 0, \end{aligned} \tag{2}$$

where T, u, and D denote the stress tensor, mechanical displacement, and electric induction vectors, respectively; ρ is the mass density of the media; c^E_{ijkl} are the elastic constants measured at constant electric field E; e_{ijk} are the piezoelectric constants; ϵ^S_{ij} are the dielectric constants measured under constant strain S; φ is the electrostatic potential: $\mathbf{E} = -\nabla\varphi$. The time-harmonic wave field is a function of $e^{-j\omega t}$, where the angular frequency ω is assumed. The time derivative in Eq. (2) is therefore: $\rho\ddot{u}_j = -\rho\omega^2 u_j$. The solution for filed components in the piezoelectric slab under crossed periodic arrays of conducting strips is sought in the form of Bloch series:

$$\begin{aligned} u_i &= \sum_{n,m} U^{(i)}_{nm} \Psi_{nm} e^{-jk_{nm}x_3}, \\ \varphi &= \sum_{n,m} \varphi_{nm} \Psi_{nm} e^{-jk_{nm}x_3}, \\ \Psi_{nm} &\equiv e^{-j(r_n x_1 + s_m x_2)} = e^{-j\xi_{nm} x^\tau_{nm}}, \end{aligned} \tag{3}$$

where Ψ_{nm} are the planar spatial harmonics defined in the plane $x_3 = 0$ parallel to strip systems. The spectrum variables r_n and s_m corresponding to the x_1 and x_2 spatial variables are defined as follows:

$$\begin{aligned} r_n &= r + nK, \qquad s_m = s + mK, \\ \xi_{nm} &= \sqrt{r_n^2 + s_m^2}, \end{aligned} \tag{4}$$

where $K = 2\pi/\Lambda$ is the wavenumber of the strip array; is the strip period (distance between the centres of adjacent strips); $r \in (0, K)$ and $s \in (0, K)$ are arbitrary spatial spectrum variables reduced to one Brillouin zone for the uniqueness of representation; ξ_{nm} is a wavenumber defined in the plane $x_3 = 0$ along the axis x^τ_{nm} rotated by the angle $\vartheta_{nm} = \tan^{-1}(s_m/r_n)$ with respect to the x_1 axis in the x_1x_2 plane: $x_1 = x^\tau_{nm}\cos\vartheta_{nm}$, $x_2 = x^\tau_{nm}\sin\vartheta_{nm}$. In Eq. (3) k_{nm} is the spectrum variable corresponding to the x_3 spatial coordinate to be defined later; and $u^{(i)}_{nm}$ and ϕ_{nm}

are the mode amplitudes for mechanical displacement and electrostatic potential, respectively. Substituting Eq. (3) into Eq. (2) and taking into account that:

$$\begin{aligned}
&\frac{\partial}{\partial x_1} = -jr_n, \quad \frac{\partial}{\partial x_2} = -js_m, \quad \frac{\partial}{\partial x_3} = -jk_{nm},\\
&\frac{\partial^2}{\partial x_1^2} = -r_n^2, \quad \frac{\partial^2}{\partial x_2^2} = -s_m^2, \quad \frac{\partial^2}{\partial x_3^2} = -k_{nm}^2,\\
&\frac{\partial^2}{\partial x_1 \partial x_2} = -r_n s_m, \quad \frac{\partial^2}{\partial x_1 \partial x_3} = -r_n k_{nm},\\
&\frac{\partial^2}{\partial x_2 \partial x_3} = -s_m k_{nm},
\end{aligned} \tag{5}$$

the Christoffel equations for all spatial harmonics can be obtained:

$$\begin{pmatrix} R_{11} & R_{12} & R_{13} & R_{14} \\ R_{21} & R_{22} & R_{23} & R_{24} \\ R_{31} & R_{32} & R_{33} & R_{34} \\ R_{41} & R_{42} & R_{43} & R_{44} \end{pmatrix} \begin{pmatrix} u_{nm}^1 \\ u_{nm}^2 \\ u_{nm}^3 \\ \varphi_{nm} \end{pmatrix} = 0. \tag{6}$$

In the particular case of piezoelectric materials having 2 mm symmetry (e.g. PZT-5H and PVDF), the coefficients of the Christoffel matrix can easily be deduced:

$$\begin{aligned}
R_{11} &= c_{11}^E r_n^2 + c_{66}^E s_m^2 + c_{44}^E k_{nm}^2 - \rho\omega^2,\\
R_{12} &= (c_{12}^E + c_{66}^E) r_n s_m,\\
R_{13} &= (c_{13}^E + c_{44}^E) r_n k_{nm},\\
R_{14} &= (e_{15} + e_{31}) r_n k_{nm},\\
R_{22} &= c_{66}^E r_n^2 + c_{22}^E s_m^2 + c_{44}^E k_{nm}^2 - \rho\omega^2,\\
R_{23} &= (c_{23}^E + c_{44}^E) s_m,\\
R_{24} &= (e_{24} + e_{32}) s_m k_{nm},\\
R_{33} &= c_{55}^E r_n^2 + c_{44}^E s_m^2 + c_{33}^E k_{nm}^2 - \rho\omega^2,\\
R_{34} &= e_{15} r_n^2 + e_{24} s_m^2 + e_{33} k_{nm}^2,\\
R_{44} &= -\varepsilon_{11}^S r_n^2 - \varepsilon_{22}^S s_m^2 - \varepsilon_{33}^S k_{nm}^2,\\
R_{ij} &= R_{ij}, \qquad i,j = 1,...,4.
\end{aligned} \tag{7}$$

In Eq. (7) the material constants are represented in contracted form to shorten notation:

$$c_{IJ}^E = \begin{pmatrix} c_{11}^E & c_{12}^E & c_{13}^E & 0 & 0 & 0 \\ c_{12}^E & c_{22}^E & c_{23}^E & 0 & 0 & 0 \\ c_{13}^E & c_{23}^E & c_{33}^E & 0 & 0 & 0 \\ 0 & 0 & 0 & c_{44}^E & 0 & 0 \\ 0 & 0 & 0 & 0 & c_{55}^E & 0 \\ 0 & 0 & 0 & 0 & 0 & c_{66}^E \end{pmatrix},$$

$$e_{iJ} = \begin{pmatrix} 0 & 0 & 0 & 0 & e_{15} & 0 \\ 0 & 0 & 0 & e_{24} & 0 & 0 \\ e_{31} & e_{32} & e_{33} & 0 & 0 & 0 \end{pmatrix},$$

$$\varepsilon_{ij}^S = \begin{pmatrix} \varepsilon_{11}^S & 0 & 0 \\ 0 & \varepsilon_{22}^S & 0 \\ 0 & 0 & \varepsilon_{33}^S \end{pmatrix},$$

where IJ are as follows: $I \to ij : 1 \to 11, 2 \to 22, 3 \to 33, 4 \to 23(32), 5 \to 13(31), 6 \to 12(21)$. The system of equations in Eq. (6) has a nontrivial solution only if the corresponding determinant of the matrix R_{ij} is equal to zero:

$$|R_{ij}(n,m)| = 0. \tag{8}$$

The determinant of matrix R_{ij} can be represented by the 8th-degree polynomial with respect to k_{nm}:

$$|R_{ij}(n,m)| = a_8 k_{nm}^8 + ... + a_1 k_{nm} + a_0 = 0,$$

in which coefficients are functions of the wave-number components and material constants. The polynomial has eight roots: $k_{nm} = k_{nmr}, r = 1,...,8$. In the case considered (lossless material and the orientation of the slab with respect to the x_3-axis), the resulting polynomial is an even function of k_{nm} ($a_j = 0$, $j = 1,3,5,7$) and all coefficients a_j are real-valued. Therefore, roots can be paired. Each pair contains either real-valued or complex conjugate roots. They represent either propagating or evanescent modes in the slab, respectively. Specifically, the roots satisfy the following condition:

$$k_{nm(2r)} = -k_{nm(2r-1)}, \quad r = 1,...,4. \tag{9}$$

Substituting the roots into Eq. (6), the modes amplitudes $U_{nmr}^{(i)}$ and φ_{nmr} can be obtained. Superposition of 8 partial waves yields the general solution for the $(n,\ m)$-th spatial harmonic:

$$\begin{aligned}
u^{(i)}(n,m) &= \sum_{r=1}^{8} (C_{nmr} U_{nmr}^{(i)}) \Psi_{nm} e^{-jk_{nmr}x_3},\\
\varphi(n,m) &= \sum_{r=1}^{8} (C_{nmr} \varphi_{nmr}) \Psi_{nm} e^{-jk_{nmr}x_3}.
\end{aligned} \tag{10}$$

Taking into account Eq. (9), the above equations can be rewritten as follows:

$$\begin{aligned}
u^{(i)}(n,m) &= \sum_{r=1}^{4} (C_{nmr}^{\pm} U_{nmr}^{(i)\pm}) \Psi_{nm} e^{\pm jk_{nmr}x_3},\\
\varphi(n,m) &= \sum_{r=1}^{4} (C_{nmr}^{\pm} \varphi_{nmr}^{\pm}) \Psi_{nm} e^{\pm jk_{nmr}x_3}.
\end{aligned} \tag{11}$$

In Eq. (11) summation is over r and the partial waves with $\pm$ signs are summed for each value of $r = 1,...,4$. There are 8 unknown constants $C_{nmr}^{\pm}$ for each $(n,\ m)$-th spatial harmonic in Eq. (11) which are determined from mechanical and electric boundary conditions.

3. Mechanical boundary conditions

In the case of thin strips deposited on the surface of a piezoelectric slab, mechanical boundary conditions may be assumed to be uniform. Specifically, the traction-free condition on the surfaces of the slab has to be satisfied:

$$T_{i3} = 0, \qquad x_3 = \pm h, \tag{12}$$

where T_{i3} are the normal stress components. Substituting Eq. (11) into the first equation in Eq. (1) and using Eq. (12) and the orthogonality of spatial harmonics, the system of linear equations for unknown coefficients $C^{\pm}_{nmr}$ can be obtained:

$$\widehat{T}_{kl}\widehat{C}_l = 0, \qquad k = 1, ..., 6, \qquad l = 1, ..., 8, \tag{13}$$

where the vector of unknown coefficients C_l is defined for the (n, m)-th spatial harmonic as follows:

$$(\widehat{C}) \equiv (C^{+}_{nmr} C^{-}_{nmr})^{\mathrm{T}}, \qquad r = 1, ..., 4, \tag{14}$$

and the elements of matrix $\widehat{T}_{kl}$ are:

$$\begin{aligned}
\widehat{T}_{1r} &= \Big(c^E_{44}(r_n U^{(3)+}_{nmr} - k_{nmr} U^{(1)+}_{nmr}) + e_{15} r_n \varphi^{+}_{nmr}\Big) A^*,\\
\widehat{T}_{1,r+4} &= \Big(c^E_{44}(r_n U^{(3)-}_{nmr} + k_{nmr} U^{(1)-}_{nmr}) + e_{15} r_n \varphi^{-}_{nmr}\Big) B^*,\\
\widehat{T}_{2r} &= \Big(c^E_{44}(s_m U^{(3)+}_{nmr} - k_{nmr} U^{(2)+}_{nmr}) + e_{15} s_m \varphi^{+}_{nmr}\Big) A^*,\\
\widehat{T}_{2,r+4} &= \Big(c^E_{44}(s_m U^{(3)-}_{nmr} + k_{nmr} U^{(2)-}_{nmr}) + e_{15} s_m \varphi^{-}_{nmr}\Big) B^*,\\
\widehat{T}_{3r} &= \Big(c^E_{13}(r_n U^{(1)+}_{nmr} + s_m U^{(2)+}_{nmr})\\
&\quad - k_{nmr}(c^E_{33} U^{(3)+}_{nmr} + e_{33}\varphi^{+}_{nmr})\Big) A^*,\\
\widehat{T}_{3,r+4} &= \Big(c^E_{13}(r_n U^{(1)-}_{nmr} + s_m U^{(2)-}_{nmr})\\
&\quad + k_{nmr}(c^E_{33} U^{(3)-}_{nmr} + e_{33}\varphi^{-}_{nmr})\Big) B^*,\\
\widehat{T}_{4r} &= \Big(c^E_{44}(r_n U^{(3)+}_{nmr} - k_{nmr} U^{(1)+}_{nmr}) + e_{15} r_n \varphi^{+}_{nmr}\Big) B^*,\\
\widehat{T}_{4,r+4} &= \Big(c^E_{44}(r_n U^{(3)-}_{nmr} + k_{nmr} U^{(1)-}_{nmr}) + e_{15} r_n \varphi^{-}_{nmr}\Big) A^*,\\
\widehat{T}_{5r} &= \Big(c^E_{44}(s_m U^{(3)+}_{nmr} - k_{nmr} U^{(2)+}_{nmr}) + e_{15} s_m \varphi^{+}_{nmr}\Big) B^*,\\
\widehat{T}_{5,r+4} &= \Big(c^E_{44}(s_m U^{(3)-}_{nmr} + k_{nmr} U^{(2)-}_{nmr}) + e_{15} s_m \varphi^{-}_{nmr}\Big) A^*,\\
\widehat{T}_{6r} &= \Big(c^E_{13}(r_n U^{(1)+}_{nmr} + s_m U^{(2)+}_{nmr})\\
&\quad - k_{nmr}(c^E_{33} U^{(3)+}_{nmr} + e_{33}\varphi^{+}_{nmr})\Big) B^*,\\
\widehat{T}_{6,r+4} &= \Big(c^E_{13}(r_n U^{(1)-}_{nmr} + s_m U^{(2)-}_{nmr})\\
&\quad + k_{nmr}(c^E_{33} U^{(3)-}_{nmr} + e_{33}\varphi^{-}_{nmr})\Big) A^*,
\end{aligned} \tag{15}$$

where

$$A^* = e^{jk_{nmr}h}, \qquad B^* = e^{-jk_{nmr}h}.$$

Mechanical boundary conditions (Eq. (12)) yield 6 equations for 8 unknown variables. The remaining equations can be obtained from the electrical boundary conditions considered below.

4. Electrical boundary conditions

For the crossed-electrode structure (see Fig. 1) electrical boundary conditions are determined by the periodic strips deposited on the opposite surfaces of the slab. Specifically, on the upper (superscript '+') and bottom (superscript '–') surfaces of the slab the components of electric field should obey the following conditions:

$$\begin{aligned}
E^{\pm}_1 = 0, \quad E^{\pm}_2 = 0, &\qquad \text{on strips},\\
\Delta D^{\pm}_3 \equiv D^{\pm} = 0, &\qquad \text{between strips}.
\end{aligned} \tag{16}$$

The boundary conditions (Eq. (16)) state that the tangential electric field vanishes on strips, and between strips the jump discontinuity of the normal component of the electric induction vector vanishes. The electrostatic potential on the slab surfaces can be expanded into Bloch series as follows:

$$\varphi^{\pm}(x_1, x_2) = \sum_{n,m} \varphi^{\pm}_{nm} \Psi_{nm}, \tag{17}$$

where Ψ_{nm} are defined in Eq. (3) and the amplitudes $\varphi^{\pm}_{nm}$ of the surface modes result directly from Eq. (11):

$$\begin{aligned}
\varphi^{+}_{nm} &= \sum_r (C^{+}_{nmr}\varphi^{+}_{nmr} e^{+jk_{nmr}h} + C^{-}_{nmr}\varphi^{-}_{nmr} e^{-jk_{nmr}h}),\\
\varphi^{-}_{nm} &= \sum_r (C^{+}_{nmr}\varphi^{+}_{nmr} e^{-jk_{nmr}h} + C^{-}_{nmr}\varphi^{-}_{nmr} e^{+jk_{nmr}h}).
\end{aligned} \tag{18}$$

Electrostatic potential, which obeys the Laplace equation outside the slab and is continuous on the boundaries $x_3 = \pm h$, can be expressed in the following form satisfying Floquet's theorem:

$$\begin{aligned}
\varphi^{a} &= \sum_{n,m} \varphi^{+}_{nm} \Psi_{nm} e^{-|\xi_{nm}|(x_3 - h)}, &\qquad x_3 > h,\\
\varphi^{b} &= \sum_{n,m} \varphi^{-}_{nm} \Psi_{nm} e^{|\xi_{nm}|(x_3 + h)}, &\qquad x_3 < -h,
\end{aligned} \tag{19}$$

where the wavenumber ξ_{nm} is defined in Eq. (4). In Eq. (19) the superscripts 'a' and 'b' denote the field variables above the slab, $x_3 > h$ and below the slab, $x_3 < -h$, respectively. The jump discontinuity of the normal electric induction $\Delta D^{\pm}_3$ is defined as follows:

$$\begin{aligned}
\Delta D^{+}_3 &= D_3(x_3 = h + 0) - D_3(x_3 = h - 0),\\
\Delta D^{-}_3 &= D_3(x_3 = -h - 0) - D_3(x_3 = -h + 0).
\end{aligned} \tag{20}$$

In Eq. (20) the normal electric induction in the slab $D^{\pm}_3$ can be obtained from Eq. (1). Specifically, for the (n, m)-th spatial harmonic amplitudes one obtains:

$$\begin{aligned}
D^{+}_{3nm} &= -j \sum_{p=1}^{4} C^{\pm}_{nmp}\Big(e_{31} r_n U^{(1)\pm}_{nmp} + e_{32} s_m U^{(2)\pm}_{nmp}\\
&\quad \mp k_{nmp}(e_{33} U^{(3)\pm}_{nmp} - \varepsilon^S_{33}\varphi^{\pm}_{nmp})\Big) e^{\pm jk_{nmp}h},\\
D^{-}_{3nm} &= -j \sum_{p=1}^{4} C^{\pm}_{nmp}\Big(e_{31} r_n U^{(1)\pm}_{nmp} + s_m e_{32} U^{(2)\pm}_{nmp}\\
&\quad \mp k_{nmp}(e_{33} U^{(3)\pm}_{nmp} - \varepsilon^S_{33}\varphi^{\pm}_{nmp})\Big) e^{\mp jk_{nmp}h}.
\end{aligned} \tag{21}$$

Equation (21) describes the normal electric induction component on the surfaces of the piezoelectric slab. Outside the slab the amplitudes of the $(n,\, m)$-th spatial harmonics of the normal electric induction are as follows:

$$D^{a,b}_{3nm} = -\varepsilon_M(\varphi^{a,b}_{,3})_{nm} = \pm\varepsilon_M|\xi_{nm}|\varphi^{\pm}_{nm}, \tag{22}$$

where the definition of electrostatic potential outside the slab (Eq. (19)) was used. In Eq. (22), ε_M is the dielectric permittivity of the medium surrounding the piezoelectric slab. Substituting Eq. (21) and Eq. (22) into Eq. (2), the jump discontinuity of the normal electric induction across the boundaries can be obtained:

$$\begin{aligned}\Delta D^{+}_{3nm} &= -j\sum_{p=1}^{4} C^{\pm}_{nmp}\Big(e_{31}r_nU^{(1)\pm}_{nmp} + e_{32}s_mU^{(2)\pm}_{nmp}\\ &\mp k_{nmp}e_{33}U^{(3)\pm}_{nmp} \pm (\varepsilon^S_{33}k_{nmp} \mp j\varepsilon_M|\xi_{nm}|)\varphi^{\pm}_{nmp}\Big)e^{\pm jk_{nmp}h},\\ \Delta D^{-}_{3nm} &= -j\sum_{p=1}^{4} C^{\pm}_{nmp}\Big(e_{31}r_nU^{(1)\pm}_{nmp} + e_{32}s_mU^{(2)\pm}_{nmp}\\ &\mp k_{nmp}e_{33}U^{(3)\pm}_{nmp} \pm (\varepsilon^S_{33}k_{nmp} \pm j\varepsilon_M|\xi_{nm}|)\varphi^{\pm}_{nmp}\Big)e^{\mp jk_{nmp}h}.\end{aligned} \tag{23}$$

Tangential components of the electric field vectors $E^{\pm}_1$ and $E^{\pm}_2$ can be obtained from the definition of electrostatic potential (Eq. (17)). Specifically, for amplitudes of the $(n,\, m)$-th harmonics one obtains:

$$E^{\pm}_{1nm} = -jr_n\varphi^{\pm}_{nm}, \qquad E^{\pm}_{2nm} = -js_m\varphi^{\pm}_{nm}. \tag{24}$$

For further analysis it is convenient to consider the tangential field component in the planes of strips $x_3 = \pm h$:

$$E^{\pm}_{\xi}(n,m) = -j\xi_{nm}\varphi^{\pm}_{nm}e^{-j\xi_{nm}x^{\tau}_{nm}}, \tag{25}$$

where

$$x_1 = x^{\tau}_{nm}\cos\vartheta_{nm}, \qquad x_2 = x^{\tau}_{nm}\sin\vartheta_{nm},$$
$$\xi^2_{nm} = r^2_n + s^2_m,$$

and the angle $\vartheta_{nm} = \tan^{-1}(s_m/r_n)$ (see Eq. (4)). For further analysis (see Sec. 5) the relation between the tangential electric field and the jump discontinuity of the normal electric induction in the planes is needed. For this purpose it is convenient to write the unknown coefficient $C^{\pm}_{nmr}$ in terms of two unknown constants to be determined from the electric boundary conditions. Specifically, by rearrangement of Eq. (13) the system of equations can be rewritten as follows:

$$\widetilde{T}_{km}\widetilde{C}_m = B_k, \qquad k,m = 1,...,6, \tag{26}$$

where

$$\widetilde{T}_{km} = \widehat{T}_{k,m+2}, \quad k,m = 1,...,6, \quad \text{and} \quad \widetilde{C}_m = \widehat{C}_{m+2}$$
$$[\widetilde{C}] \equiv [C^{+}_{nm,p+1}C^{-}_{nm,p+1}]^{\mathrm{T}}, \quad p = 1,...,3. \tag{27}$$

The elements of vector B in Eq. (26) are defined as follows:

$$B_k = \overline{T}_{ki}A_i, \qquad k = 1,...,6, \qquad i = 1,2, \tag{28}$$

where $\overline{T}_{ki} = T_{ki}$, $k = 1,...,6$, $i = 1,2$. In Eq. (28) a new vector $A_i \equiv A_{inm}$, $i = 1,2$ was introduced for each spatial harmonics as follows:

$$[A] = [A_{1nm}A_{2nm}]^{\mathrm{T}} \equiv [C^{+}_{nm1}C^{-}_{nm1}]^{\mathrm{T}}. \tag{29}$$

It is clear that six out of eight unknown coefficients $C^{\pm}_{nmp}$, defined in Eq. (27), can be obtained as a linear combination of the remaining two coefficients $C^{\pm}_{nm1}$ in Eq. (31), which is redefined for convenience as follows:

$$[\widetilde{C}] = [\widetilde{T}]^{-1}[\overline{T}][A] = [\widetilde{a}][A]. \tag{30}$$

For further analysis it is convenient to rewrite Eq. (30) in a slightly different form:

$$[\widehat{C}] = [\widehat{a}][A], \tag{31}$$

The elements of matrix $[\widehat{a}]$ in Eq. (31) are given by the following expressions:

$$\begin{aligned}&a_{11} = 1, \quad a_{12} = 0; \qquad a_{21} = 0, \quad a_{22} = 1,\\ &a_{k+2,i} = a_{ki}, \qquad k = 1,...,6, \qquad i = 1,2,\end{aligned} \tag{32}$$

and

$$[\widetilde{a}] = [\widetilde{T}]^{-1}[\overline{T}]. \tag{33}$$

In Eq. (33) $\widetilde{T}_{ki} = \widehat{T}_{k,i+2}$, $k,i = 1,...,6$, and $\overline{T}_{kj} = \widehat{T}_{kj}$, $k = 1,...,6$, $j = 1,2$. The elements of matrix $\widehat{T}_{ki}$ are defined in Eq. (15). Equations (30) through (33) hold for each spatial harmonic $(n,\, m)$. To emphasize this and to simplify further analysis it is convenient to rewrite the elements $\widehat{a}_{ij}$ as follows:

$$\begin{aligned}&\widehat{a}^{i+}_{nmp} \equiv \widehat{a}_{2p-1,i}, \qquad \widehat{a}^{i-}_{nmp} \equiv \widehat{a}_{2p,i},\\ &i = 1,2; \qquad p = 1,...,4.\end{aligned} \tag{34}$$

It should be noted that only two out of eight coefficients $(C^{\pm}_{nmn})$ defined in Eq. (31) remain unknown. They can be determined from the electric boundary conditions. Using Eq. (31), the mode amplitudes of the electric potentials on the boundaries $x_3 = \pm h$ defined in Eq. (18) can be rewritten as follows:

$$\begin{pmatrix}\widehat{\varphi}^{+}_{nm}\\ \widehat{\varphi}^{-}_{nm}\end{pmatrix} = \begin{pmatrix}L^{1+}_{nm} & L^{2+}_{nm}\\ L^{1-}_{nm} & L^{2-}_{nm}\end{pmatrix}\begin{pmatrix}A_{1nm}\\ A_{2nm}\end{pmatrix}. \tag{35}$$

In Eq. (35) matrix notation was used for brevity. The elements of matrix $L^{i\pm}_{nm}$ are defined as follows:

$$L^{i\pm}_{nm} = \sum_{p=1}^{4}(\widehat{a}^{i+}_{nmp}\varphi^{+}_{nmp}e^{\pm jk_{nmp}h} + \widehat{a}^{i-}_{nmp}\varphi^{-}_{nmp}e^{\mp jk_{nmp}h}), \tag{36}$$

where the coefficients $\widehat{a}^{i+}_{nmp}$ result directly from Eq. (36). Similarly, the mode amplitudes of the $(n,\ m)$-th spatial harmonic of the tangential electric field $E^{\pm}_{\xi nm}$ can be written as follows:

$$\begin{pmatrix} E^{+}_{\xi nm} \\ E^{-}_{\xi nm} \end{pmatrix} = -j\xi_{nm} \begin{pmatrix} L^{1+}_{nm} & L^{2+}_{nm} \\ L^{1-}_{nm} & L^{2-}_{nm} \end{pmatrix} \begin{pmatrix} A_{1nm} \\ A_{2nm} \end{pmatrix}. \tag{37}$$

Finally, for the jump discontinuity of the normal electric induction defined in Eq. (23), it can be rewritten in the following form:

$$\begin{pmatrix} \Delta D^{+}_{3nm} \\ \Delta D^{-}_{3nm} \end{pmatrix} = -j \begin{pmatrix} M^{1+}_{nm} & M^{2+}_{nm} \\ M^{1-}_{nm} & M^{2-}_{nm} \end{pmatrix} \begin{pmatrix} A_{1nm} \\ A_{2nm} \end{pmatrix}, \tag{38}$$

where the elements of matrix $M^{i\pm}_{nm}$ are:

$$\begin{aligned} M^{i\pm}_{nm} &= \sum_{p=1}^{4} \widehat{a}^{i+}_{nmp} \Big(e_{31} r_n U^{(1)+}_{nmp} + e_{32} s_m U^{(2)+}_{nmp} \\ &- k_{nmp} e_{33} U^{(3)+}_{nmp} + (\varepsilon^{S}_{33} k_{nmp} \mp j\varepsilon_M |\xi_{nm}|) \varphi^{\pm}_{nmp} \Big) e^{\pm j k_{nmp} h} \\ &+ \sum_{p=1}^{4} \widehat{a}^{i-}_{nmp} \Big(e_{31} r_n U^{(1)-}_{nmp} + e_{32} s_m U^{(2)-}_{nmp} \\ &+ k_{nmp} e_{33} U^{(3)-}_{nmp} - (\varepsilon^{S}_{33} k_{nmp} \pm j\varepsilon_M |\xi_{nm}|) \varphi^{\pm}_{nmp} \Big) e^{\mp j k_{nmp} h}. \end{aligned} \tag{39}$$

From Eqs (37) and (38) the relationship between the tangential electric field and the normal electric induction on the boundary surfaces of piezoelectric slab can be obtained immediately:

$$[E_\xi] = \xi_{nm} [G] [\Delta D_3], \tag{40}$$

where

$$[E_\xi] = [E^{+}_{\xi nm} E^{-}_{\xi nm}]^{\mathrm{T}}, \qquad [\Delta D_3] = [\Delta D^{+}_{3nm} \Delta D^{-}_{3nm}]$$

and the matrix $[G]$ is defined as follows:

$$[G] = [L][M]^{-1}. \tag{41}$$

5. Electrostatic field approximation

To obey the electrical boundary conditions and find the unknown coefficients A_{inm}, $i = 1, 2$ in Eq. (29) the tangential electric field and normal electric induction in the boundary plane $x_3 = h$ can be rewritten in the form of series expansion as follows (Danicki, 2010):

$$\begin{aligned} E^{+}_{1} &= j \sum_{l,n,m} \alpha^{m}_{l} S_{n-l} P_{n-l}(\Delta) \Psi_{nm}, \\ E^{+}_{2,1} &= j \sum_{l,n,m} \alpha^{m}_{l} S_{n-l} P_{n-l}(\Delta) \Psi_{nm}, \\ \Delta D^{+}_{3} &= \sum_{l,n,m} \beta^{m}_{l} P_{n-l}(\Delta) \Psi_{nm}, \end{aligned} \tag{42}$$

and in the plane $x_3 = -h$:

$$\begin{aligned} E^{-}_{2} &= j \sum_{l',n,m} \gamma^{n}_{l'} S_{m-l'} P_{m-l'}(\Delta) \Psi_{nm}, \\ E^{-}_{1,2} &= j \sum_{l',n,m} \gamma^{n}_{l'} S_{m-l'} P_{m-l'}(\Delta) \Psi_{nm} \\ \Delta D^{-}_{3} &= \sum_{l',n,m} \eta^{n}_{l'} P_{m-l'}(\Delta) \Psi_{nm}, \end{aligned} \tag{43}$$

where $\Delta = \cos(\pi w/\Lambda)$, $P_k(\cdot)$ are the Legendre polynomials, $S_\nu = 0$ for $\nu < 0$ and $S_\nu = 1$ otherwise, and w is the strip's width. The above expansions yield the electric field satisfying boundary conditions, Eq. (16), and the edge conditions. Specifically, the normal electric induction ΔD^{+}_{3} and tangential electric field E^{+}_{1} are inverse square-root singular functions at the edges of strips located in the plane $x_3 = h$. The E^{+}_{2} component is not singular, but its spatial derivative with respect to x_1 has an inverse square-root singularity at the strip edges as well. Therefore, in Eq. (42) the corresponding series expansion of $E^{+}_{2,1}$ is introduced. The bottom boundary can be handled similarly, but in this case ΔD^{-}_{3}, E^{-}_{2}, and $E^{-}_{1,2}$ are singular functions and the corresponding series expansions are introduced in Eq. (43). In Eqs (42) and (43) α^{m}_{l}, $\widetilde{\alpha}^{m}_{l}$, β^{m}_{l}, $\gamma^{n}_{l'}$, $\widetilde{\gamma}^{n}_{l'}$, and $\eta^{n}_{l'}$ are unknown expansion coefficients. Using Eq. (24) it can be shown that the following relations hold:

$$\widetilde{\alpha}^{m}_{l} = -j s_m \alpha^{m}_{l}, \qquad \widetilde{\gamma}^{n}_{l'} = -j r_n \gamma^{n}_{l'}. \tag{44}$$

The remaining coefficients α^{m}_{l}, β^{m}_{l}, $\gamma^{n}_{l'}$, and $\eta^{n}_{l'}$ can be obtained using Eq. (40) which yields the relationship between the tangential electric field and the normal electric induction on the upper and bottom boundaries. Components of the tangential electric field in the planes of strips can be written as follows:

$$E^{+}_{\xi nm} = \frac{\xi_{nm}}{r_n} E^{+}_{1nm}, \qquad E^{-}_{\xi nm} = \frac{\xi_{nm}}{s_m} E^{-}_{2nm}. \tag{45}$$

Consequently, the corresponding series expansions for tangential field components can be written as follows:

$$\begin{aligned} E^{+}_{\xi} &= j \sum_{l,n,m} \frac{\xi_{nm}}{r_n} \alpha^{m}_{l} S_{n-l} P_{n-l}(\Delta) \Psi_{nm}, \\ E^{-}_{\xi} &= j \sum_{l',n,m} \frac{\xi_{nm}}{s_m} \gamma^{n}_{l'} S_{m-l'} P_{m-l'}(\Delta) \Psi_{nm}. \end{aligned} \tag{46}$$

Further analysis is based on approximation of matrix $[G]$ in Eq. (40) for large indices (n, m) corresponding to imaginary-valued k_{nmp} with spatial harmonics well-localized at a given surface of piezoelectric slab. Specifically, it can be shown that for (n, m) sufficiently large, matrix $[G]$ can be approximated as:

$$\begin{pmatrix} E^{+}_{\xi NM} \\ E^{-}_{\xi NM} \end{pmatrix} \approx j S_{NM} \begin{pmatrix} (\varepsilon^{+}_{\infty})^{-1} & 0 \\ 0 & -(\varepsilon^{-}_{\infty})^{-1} \end{pmatrix} \begin{pmatrix} \Delta D^{+}_{3NM} \\ \Delta D^{-}_{3NM} \end{pmatrix}, \tag{47}$$

where $S_{NM} \equiv S_N S_M$, N and M being large but finite integers, and $S_\nu = 0$ for $\nu < 0$ and $S_\nu = 1$ otherwise. In Eq. (47) $\varepsilon^{\pm}_{\infty}$ can be obtained from Eq. (41) by accounting for Eq. (37) through Eq. (39) upon substituting the approximation $k_{nmp} \approx -j|\xi_{nm}|$, which holds for sufficiently large indices (n, m):

$$\varepsilon^{\pm}_{\infty} = (\varepsilon_{33} + \varepsilon_M) - \alpha^{\pm}_3 e_{33} \pm j(e_{31}\alpha^{\pm}_1 + e_{32}\alpha^{\pm}_2). \tag{48}$$

The coefficients $\alpha^{\pm}_i$ result from the asymptotic analysis of the wave mode amplitudes of the mechanical displacement $U^{(i)\pm}_{nmp}$ and electrostatic potential $\varphi^{\pm}_{nmp}$:

$$\alpha^{\pm}_i = \lim_{n,m\to\infty} \left(\frac{\sum_{p=1}^{4} U^{(i)\pm}_{nmp}}{\sum_{p=1}^{4} \varphi^{\pm}_{nmp}} \right), \tag{49}$$

and can be obtained numerically for given material constants of the piezoelectric slab. In the considered case of lossless material Eq. (48) can be simplified. Specifically, if Eq. (9) holds, it can be checked by inspection that coefficients $\alpha^{\pm}_1$ and $\alpha^{\pm}_2$ take imaginary values and $\alpha^{\pm}_3$ is real-valued. Moreover, $\alpha^{-}_j = -\alpha^{+}_j$, $j = 1, 2$ and $\alpha^{+}_3 = \alpha^{-}_3$. Then, from Eq. (48) it follows that $\varepsilon^{-}_{\infty} = \varepsilon^{+}_{\infty} = \varepsilon_{\infty}$.

For $n > N$ and $m > M$ where N, M are large but finite integers, such that the approximation in Eq. (47) holds, the following relationships between the expansion coefficients α^m_l and β^m_l, and $\gamma^n_{l'}$ and $\eta^n_{l'}$ can be deduced:

$$\beta^m_l = \frac{\xi_{nm}}{r_n}\varepsilon^{+}_{\infty} S_{n-l}\alpha^m_l, \quad \eta^n_{l'} = -\frac{\xi_{nm}}{s_m}\varepsilon^{-}_{\infty} S_{m-l'}\gamma^n_{l'}. \tag{50}$$

Taking into account Eq. (50) and substituting Eqs (42), (43), and (45) for the spatial harmonics with indices $-N < n < N$ and $-M < m < M$ into Eq. (40), the following system of linear equations for unknown expansion coefficients α^m_l, $-N \le l \le N$, and $\gamma^n_{l'}$, $-M \le l' \le M$ can be obtained:

$$\begin{aligned} &\alpha^m_l \left[j\frac{\xi_{nm}}{|\xi_{nm}|} - G_{11}\varepsilon^{+}_{\infty} \right] S_{n-l}P_{n-l} \\ &\qquad + \gamma^n_{l'} G_{12} \left(\frac{r_n}{s_m} \right) \varepsilon^{-}_{\infty} S_{m-l'}P_{m-l'} = 0, \\ &-\alpha^m_l G_{21} \left(\frac{s_m}{r_n} \right) \varepsilon^{+}_{\infty} S_{n-l}P_{n-l} \\ &\qquad + \gamma^n_{l'} \left[j\frac{\xi_{nm}}{|\xi_{nm}|} + G_{22}\varepsilon^{-}_{\infty} \right] S_{m-l'}P_{m-l'} = 0, \end{aligned} \tag{51}$$

where $P_\nu \equiv P_\nu(\Delta)$ was applied to shorten notation. Applying (n, m) outside the chosen domains results in a trivial solution for the additionally included unknowns. To obtain unique solution for unknown coefficients α^m_l, $\gamma^n_{l'}$, additional constraints must be fulfilled. For example, without loss of generality, it is convenient to apply the electric potential or voltage of the individual strips:

$$\begin{aligned} V(x_1 = i\Lambda) &= V_i, \qquad x_3 = h, \\ V(x_2 = j\Lambda) &= V_j, \qquad x_3 = -h. \end{aligned} \tag{52}$$

Strip voltages can be evaluated by integration of the tangential electric field, their integration being performed for each spatial harmonic separately. For a strip placed at $x_1 = 0$ (on the upper surface) and $x_2 = 0$ (on the bottom surface) they are:

$$\begin{aligned} V^{+} &= -\int E^{+}_1 dx_1 = \alpha^m_l \frac{\sum_n S_{n-l}P_{n-l}(\Delta)}{jr_n} = V(r), \\ V^{-} &= -\int E^{-}_2 dx_2 = \gamma^n_{l'} \frac{\sum_m S_{m-l'}P_{m-l'}(\Delta)}{js_m} = 0, \end{aligned} \tag{53}$$

where for simplicity the bottom strips are assumed grounded. The summation with respect to n and m in Eq. (53) can be evaluated explicitly using the Dougall identity (Erdelyi *et al.*, 1953). For instance, assuming all bottom electrodes are grounded and only a single l-th electrode on the upper surface is connected to the voltage supply V_l (note $s = 0$, $s_m = mK$ in this case) yields:

$$\begin{aligned} (-1)^l \alpha^m_l P_{-l-\frac{r}{K}}(-\Delta) &= j\delta_{m0}\frac{K}{\pi} V_l e^{jrl\Lambda} \sin\frac{\pi r}{K}, \\ (-1)^{l'} \gamma^n_{l'} P_{-l'-\frac{s}{K}}(-\Delta) &= 0, \end{aligned} \tag{54}$$

for all (n, m) accounted for in Eq. (52). In Eq. (54) δ_{ij} is the Kronecker delta. Equations (51) and (54) yield the closed system of linear equations for unknown expansion coefficients α^m_l and $\gamma^n_{l'}$. Specifically, there are $(2N+1)(2M+1)$ equations altogether and the same number of unknowns α^m_l, $\gamma^n_{l'}$, assuming $-N \le l \le N$ and $-M \le l' \le M$. Once the system of equations for α^m_l, $\gamma^n_{l'}$, is solved, the unknown constants A_{inm}, $i = 1, 2$ defined in Eq. (29) can be obtained from Eq. (37) by accounting for Eq. (45), which yields the (n, m)-th spatial harmonics:

$$\begin{pmatrix} A_{1nm} \\ A_{2nm} \end{pmatrix} = -\begin{pmatrix} L^{1+}_{nm} & L^{2+}_{nm} \\ L^{1-}_{nm} & L^{2-}_{nm} \end{pmatrix}^{-1} \begin{pmatrix} r_n^{-1} \sum_l \alpha^m_l S_{n-l}P_{n-l} \\ s_m^{-1} \sum_{l'} \gamma^n_{l'} S_{m-l'}P_{m-l'} \end{pmatrix}, \tag{55}$$

where

$$P_\nu \equiv P_\nu(\Delta).$$

Solving Eq. (55) yields the constants A_{inm}, $i = 1, 2$ and therefore all unknown constants $C^{\pm}_{nmp}$ for each spatial harmonics from Eq. (31).

6. Numerical example

To illustrate the method a simple numerical example is considered in this section. Specifically, it is

assumed that a single electrode on the upper surface is connected to the voltage source and the remaining electrodes are grounded. All electrodes on the bottom surface are assumed grounded as well (see Eqs (52) through Eq. (54)). Evaluation of the normal stress component $T_{33}(x_1, x_2, 0)$ in the plane $x_3 = 0$ is shown in the examples below to illustrate the stress distribution in piezoelectric slab within a single active transducer cell. Numerical simulations were conducted for piezoelectric material of the 2 mm symmetry class. Specifically, in the numerical example below the material properties of PZ-26 ceramics (the same material was also used later in experimental measurements, see the next Section) were used (Meggit, 2019):

- $c_{11}^E = c_{22}^E = 16.8 \cdot 10^{10}$ N/m^2,
  $c_{33}^E = 12.3 \cdot 10^{10}$ N/m^2,
  $c_{44}^E = c_{55}^E = 3.01 \cdot 10^{10}$ N/m^2,
  $c_{66}^E = 2.88 \cdot 10^{10}$ N/m^2,
  $c_{12}^E = 11.0 \cdot 10^{10}$ N/m^2,
  $c_{13}^E = c_{23}^E = 9.99 \cdot 10^{10}$ N/m^2;
- $\varepsilon_{11}^S = \varepsilon_{22}^S = 1190 \cdot \varepsilon_0$,
  $\varepsilon_{33}^S = 1330 \cdot \varepsilon_0$,
  $\varepsilon_0 = 8.85 \cdot 10^{-12}$ F/m;
- $e_{24} = e_{15} = 9.86$ C/m^2,
  $e_{31} = e_{32} = -2.8$ C/m^2,
  $e_{33} = 14.7$ C/m^2;
  $\rho = 7700$ kg/m^3.

In Fig. 2 the spatial distribution of the normal stress component $T_{33}(x_1, x_2, 0)$ for different values of w/Λ are shown (w is strip width, Λ is strip period, and the piezoelectric slab thickness is $h = \Lambda$).

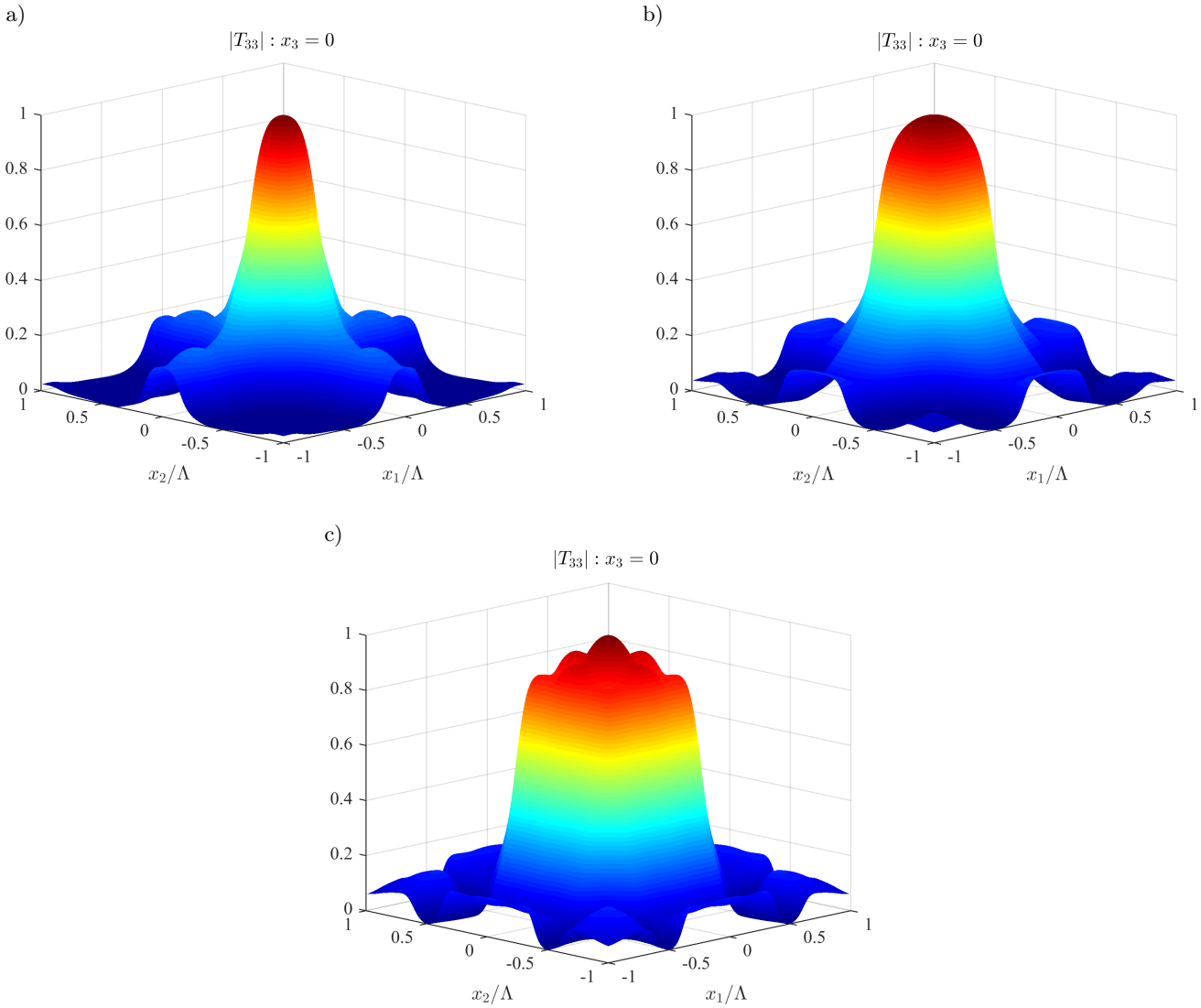

Fig. 2. Spatial distribution of the normal stress component $T_{33}(x_1, x_2)$ in the plane $x_3 = 0$ for different w/Λ: a) $\frac{w}{\Lambda} = 0.25$, b) $\frac{w}{\Lambda} = 0.5$, c) $\frac{w}{\Lambda} = 0.75$; $h = \Lambda$.

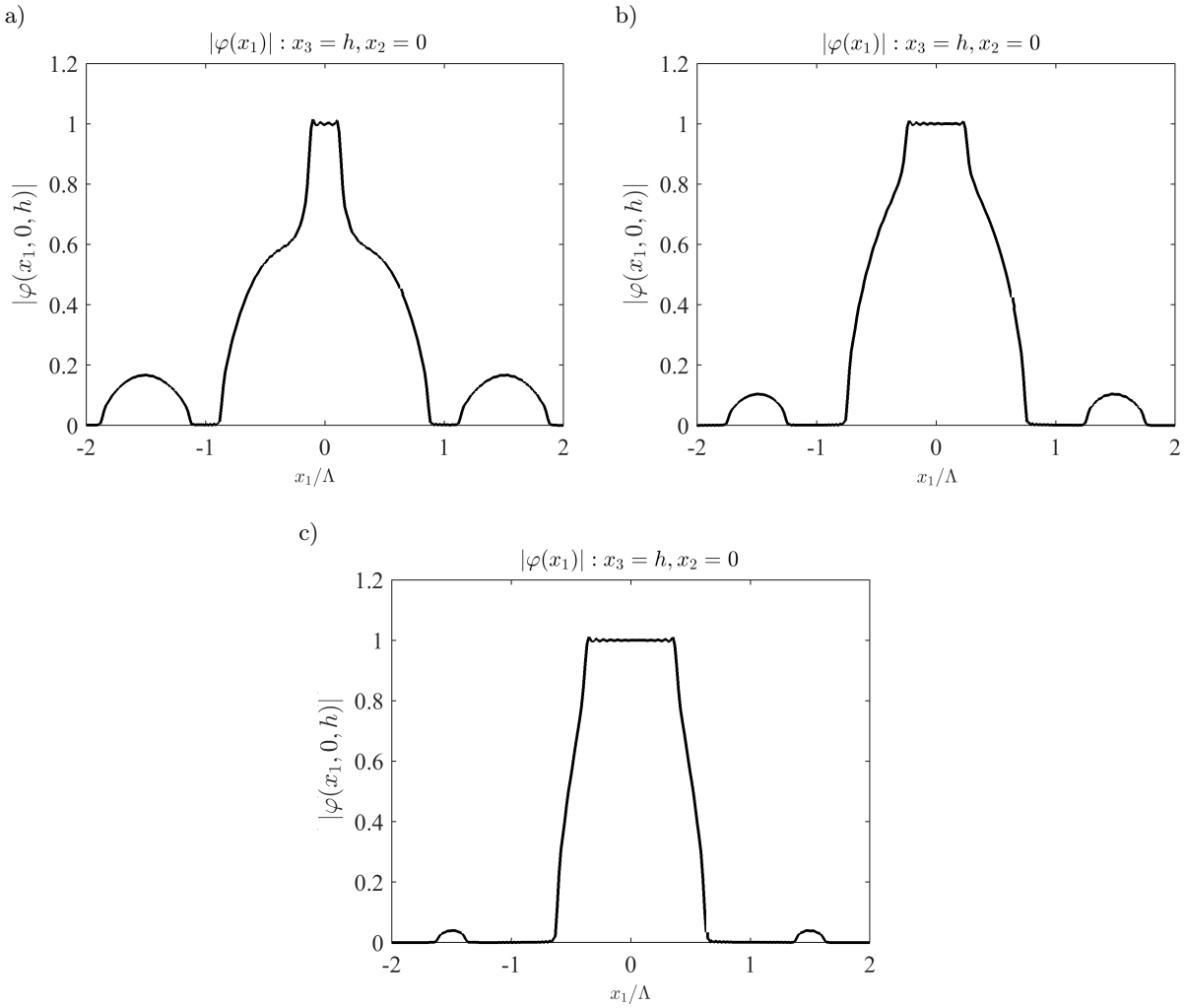

Fig. 3. Spatial distribution of electrostatic potential $\varphi(x_1)$ in the plane of the strips $x_3 = h$ for different values of w/Λ: a) $\frac{w}{\Lambda} = 0.25$, b) $\frac{w}{\Lambda} = 0.5$, c) $\frac{w}{\Lambda} = 0.75$; $h = \Lambda$.

In Fig. 3 the spatial distribution of electric potential in the plane of strips $x_3 = h$ is shown. This can be obtained by integration of the tangential electric field component in the plane of the strips (see Eq. (53)).

As can be seen from Fig. 3, electric potential is constant on strips in accordance with boundary conditions given in Eq. (52). Evaluation of potential distribution on strips allows checking if the field components were evaluated correctly.

7. Pilot experiment

In this chapter to illustrate the capabilities of the proposed arrangement of top orthogonal to bottom arrays of conducting strips a simple pilot experiment was carried out. For this purpose a test transducer was designed and made using PZ-26 ceramic layer measuring $30 \times 30 \times 0.5$ mm (produced by Meggit (2019)) polarized in the normal direction to the metallized surfaces. 64-element orthogonal array patterns were made by cutting the diamond saw on both surfaces of the layer (Fig. 4a). The strips width was 0.2 mm, the pitch was 0.2 mm yielding the period of the array pattern of 0.4 mm. The transducer was placed in a plexiglass casing (Fig. 4b). The transducer was loaded at the back with a layer made of resin (epidian) mixed with wolfram in a weight ratio of 1 to 2.

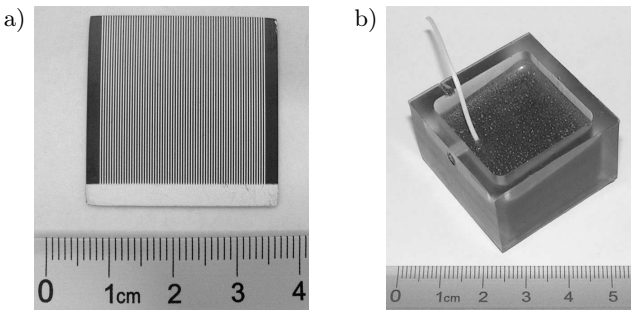

Fig. 4. (a) Array pattern of the test transducer – piezoelectric plate with strips made by cutting the diamond saw on both surfaces and (b) the transducer in plexiglass casing, covered with loading layer made of resin (epidian) mixed with wolfram.

The real view of the experimental setup is shown in Fig. 5.

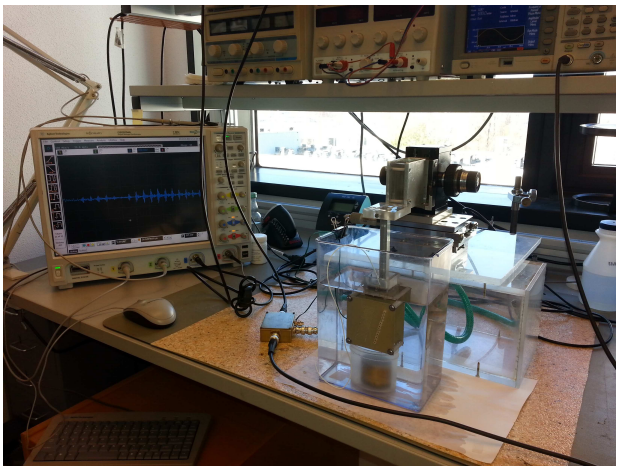

Fig. 5. Experimental setup (real view) for measuring the transmitted and back-scattered field acoustic field.

7.1. Transmitted acoustic field measurements

First, the transmitted acoustic field measurements were conducted. That was done in experimental set-up shown in Fig. 6. The transducer was immersed in water tank and connected to the Tektronix AFG 3252 signal generator. The transducer was stimulated by 10 periods of a 3.5 MHz sinusoidal signal. The excitation voltage was applied to 4 electrodes on the upper surface (el. no. 31, 32, 33, 34) connected in parallel to increase the energy of the emitted pulse. The remaining electrodes on the upper surface and all the electrodes on the bottom surface were grounded. This connection scheme is analogous to the numerical experiment considered in the previous section. The signal emitted was measured with a needle hydrophone immersed in water at a distance of 2 cm from the transducer. Between each measurement, the hydrophone was moved every 0.5 mm in the direction perpendicular to the active strips, which corresponds to an angle change of about 1.18°. The signal measured with the hydrophone was recorded with an oscilloscope DSO9104A, Keysight 366 Technologies Inc. The sampling rate was 400 MHz.

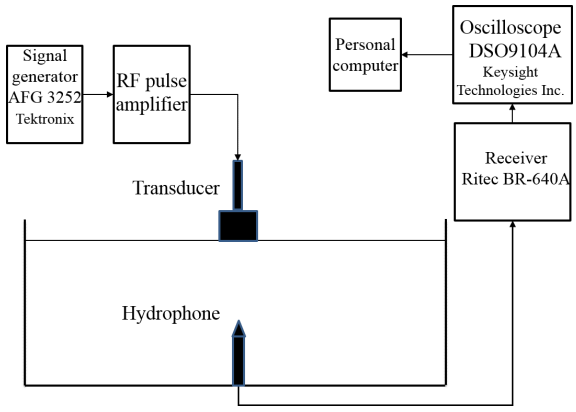

Fig. 6. Experimental setup for measuring the transmitted acoustic field of the test transducer.

The signal measured with the hydrophone is shown in Fig. 7a, while in Fig. 7b the measured far-field directivity function of the test transducer is shown. For comparison, the simulated directivity function approximated by the spatial spectrum of the normal displacement velocity in the plane of active strips (Tasinkevych, Danicki, 2011) is shown by the dashed line in Fig. 7b. The spectrum can be obtained using FFT algorithm applied to spatial distribution of the normal displacement velocity component in the plane of active strips $v_3 = -j\omega u_3$, where u_3 is given by Eq. (3) and Eq. (11).

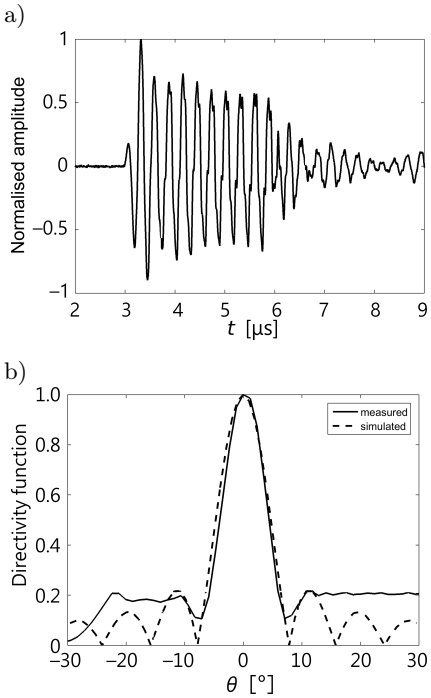

Fig. 7. Signal recorded by the hydrophone (a) and directivity function (b) of the test transducer.

7.2. Back-scattered acoustic field measurements

Moreover, the backscattered field measurements were also conducted. For this purpose a thin nylon wire of 0.1 mm in diameter was used as a point reflector. The wire was oriented in parallel direction to the active strips as illustrated in Fig. 8. The transducer was stimulated by a short pulse of 1 period of a sinusoidal signal with a frequency of 3.5 MHz. Next, the transducer was switched into the reception mode and the backscattered signal was recorded. The transducer was moved between subsequent measurements with a step of 0.1 mm in the normal direction to the active electrodes. 64 measurements were made altogether yielding 64 scanlines of the corresponding B-mode image (see Fig. 9).

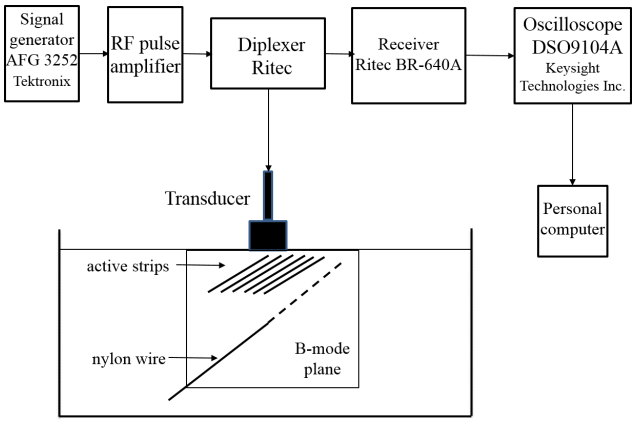

Fig. 8. Experimental setup for measuring the back-scattered acoustic field of the test transducer.

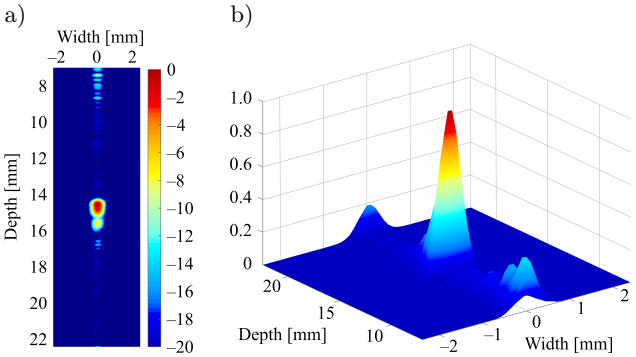

Fig. 9. Back-scattered field of the test transducer for nylon wire simulating a point reflector (a) B-mode image and (b) surface plot.

The transducer was moved between subsequent measurements with a step of 0.1 mm in the normal direction to the active electrodes. 64 measurements were conducted yielding 64 scanlines of the B-mode image, shown in Fig. 9a over 20 dB dynamic range. In Fig. 9b a surface plot of the resulting image is shown.

8. Conclusions

In this study theoretical analysis of the top orthogonal to bottom arrays of conducting strips residing on the opposite surfaces of piezoelectric dielectric slab was presented. It has been demonstrated in several studies that such row-column addressable technologies can be a low-cost alternative to the state-of-the-art fully sampled matrix transducers (Schau, 1991; Yen *et al.*, 2009). One possible application of such system is for acoustic wave generation and detection in ultrasound imaging. Rigorous electric and acoustic field analysis is usually necessary for designing and evaluating electrical and mechanical properties of such devices. For the sake of clarity strip parameters were the same on both sides of the dielectric piezoelectric slab. The method can easily be generalized for different strip periods and widths. The key point of the method is the expansion of the amplitudes of the Bloch components into appropriate series of Legendre functions. This allows the boundary conditions for electric field components on both surfaces of the piezoelectric slab to be satisfied directly. Another important feature of the method is that the singular electric field behaviour near the edges of the strips is taken into account explicitly by virtue of the form of the expansion coefficients. The main disadvantage of the presented analysis is its complexity. Nevertheless, the analysis carried out here presents a solution to the significant problem of the theory of piezoelectric devices. The results of theoretical analysis presented seem to be well suited and may be helpful in practical modelling and design of the edge-connected row-column addressable 2D transducers. This is illustrated by a simple numerical example yielding non-uniform distribution of electric field and normal stress induced in the area of the excited matrix cell for one upper strip excited by a uniform voltage and all bottom strips grounded.

Acknowledgment

This work was supported by the Polish Ministry of Science and Higher Education (Grant NO. N515 500540).

References

1. (Meggit 2019), Meggitt Vibro-MeterR homepage, http://www.meggittsensingsystems.com/.
2. Bausk E., Kolosovsky E., Kozlov A., Solie L. (2002), Optimization of broadband uniform beam profile interdigital transducers weighted by assignment of electrode polarities, *IEEE Transactions on Ultrasonics, Ferroelectrics, and Frequency Control*, **49**(1): 1–10, doi: 10.1109/58.981378.
3. Biryukov S., Polevoi V. (1996), The electrostatic problem for SAW interdigital transducers in external electric field – part I: a general solution for a limited number of electrodes, *IEEE Transactions on Ultrasonics, Ferroelectrics, and Frequency Control*, **43**(6): 1150–1159, doi: 10.1109/58.542059.
4. Blotekjar K., Ingebrigtsen K.A., Skeie H. (1973), A method for analyzing waves in structures consisting of metal strips on dispersive media, *IEEE Transactions on Electron Devices*, **20** (12): 1133–1138, doi: 10.1109/ T-ED.1973.17806.
5. Chen R. *et al.* (2014), PMN-PT single-crystal high-frequency kerfless phased-array, *IEEE Transactions on Ultrasonics, Ferroelectrics, and Frequency Control*, **61**(6): 1033–1041, doi: 10.1109/ TUFFC.2014.2999.
6. Daniau W., Kumar A.K.S., Paruch P., Marre D., Triscone J.-M., Ballandras S. (2004), A novel piezoelectric interdigital transducer for the excitation of high frequency surface acoustic waves, *IEEE Ultrasonics Symposium, 2004*, Vol. 1, pp. 441–444., doi: 10.1109/ULTSYM.2004.1417757.

7. Danicki E. (1996), Strips electrostatics – spectral approach, *1996 IEEE Ultrasonics Symposium. Proceedings*, Vol. 1, pp. 193–196, doi: 10.1109/ULTSYM.1996.583957.

8. Danicki E., Nowicki A., Tasinkevych Y. (2013), Interdigitated interdigital transducer for surface elastometry of soft damping tissue, *IEEE Transactions on Ultrasonics, Ferroelectrics, and Frequency Control*, **60**(6): 1260–1262, doi: 10.1109/TUFFC.2013.2690.

9. Danicki E.J. (2010), Electrostatics of crossed arrays of strips, *IEEE Transactions on Ultrasonics, Ferroelectrics, and Frequency Control*, **57**(7): 1701–1705, doi: 10.1109/TUFFC.2010.1601.

10. Erdelyi A., Magnus W., Oberhettinger F., Tricomi F.G. (1953), *Higher transcendental functions*, Vol. 1, New York: McGraw-Hill, http://apps.nrbook.com/bateman/Vol1.pdf.

11. Fissi L.E., Jaouad A., Vandormael D., Francis L.A. (2015), Fabrication of new Interdigital transducers for surface acoustic wave device, *Physics Procedia*, **70**: 936–940, doi: 10.1016/j.phpro.2015.08.194.

12. Morgan D.P. (1999), Quasi-static analysis of floating-electrode unidirectional SAW transducers (FEUDTs), *1999 IEEE Ultrasonics Symposium. Proceedings. International Symposium (Cat. No. 99CH37027)*, Vol. 1, pp. 107–111, doi: 10.1109/ULTSYM.1999.849366.

13. Na J.K., Blackshire J.L., Kuhr S. (2008), Design, fabrication, and characterization of single-element interdigital transducers for NDT applications, *Sensors and Actuators A: Physical*, **148**(2): 359–365, doi: 10.1016/j.sna.2008.08.018.

14. Nguyen V.H., Richert S., Park H., Böker A., Schnakenberg U. (2017), Single interdigital transducer as surface acoustic wave impedance sensor, *Procedia Technology*, **27**: 70–71, doi: 10.1016/j.protcy.2017.04.032.

15. Peach R.C. (1981), A general approach to the electrostatic problem of the SAW interdigital transducer, *IEEE Transactions on Sonics and Ultrasonics*, **28**(2): 96–104, doi: 10.1109/T-SU.1981.31227.

16. Schau H.C. (1991), Edge-connected, crossed-electrode array for two-dimensional projection and beam forming, *IEEE Transactions on Signal Processing*, **39**(2): 289–297, doi: 10.1109/78.80811.

17. Senveli S.U., Tigli O. (2015), A novel surface acoustic wave sensor for microparticle sensing and quantification, *IEEE Sensors Journal*, **15**(10): 5748–5754, doi: 10.1109/JSEN.2015.2446491.

18. Seo C.H., Yen J.T. (2009), A 256×256 2-D array transducer with row-column addressing for 3-D rectilinear imaging, *IEEE Transactions on Ultrasonics, Ferroelectrics, and Frequency Control*, **56**(4): 837–847, doi: 10.1109/TUFFC.2009.1107.

19. Tasinkevych Y., Danicki E. (2011), Wave generation and scattering by periodic baffle system in application to beam-forming analysis, *Wave Motion*, **48**(2): 130–145, doi: 10.1016/j.wavemoti.2010.10.002.

20. Wang W., Oh H., Lee K., Yoon S., Yang S. (2009), Enhanced sensitivity of novel surface acoustic wave microelectromechanical system-interdigital transducer gyroscope, *Japanese Journal of Applied Physics*, **48**(6): 06FK09, doi: 10.1143/jjap.48.06fk09.

21. White R.M., Voltmer F.M. (1965), Direct piezoelectric coupling to surface elastic waves, *Applied Physics Letters*, **7** (12): 314–316, doi: 10.1063/1.1754276.

22. Yen J.T., Seo C.H., Awad S.I., Jeong J.S. (2009), A dual-slab transducer array for 3-D rectilinear imaging, *IEEE Transactions on Ultrasonics, Ferroelectrics, and Frequency Control*, **56**(1): 204–212, doi: 10.1109/TUFFC.2009.1020.